Optics Letters

Spin-orbital angular momentum tomography of a chiral plasmonic lens using leakage radiation microscopy

Airong Zhao,[1,2,3] Aline Pham,[1] Nessim Jebali,[1] and Aurélien Drezet[1,*]

[1]Institut NEEL, CNRS and Université Grenoble Alpes, Grenoble 38000, France
[2]Changchun Institute of Optics, Fine Mechanics and Physics, Chinese Academy of Sciences, Changchun 130033, China
[3]University of Chinese Academy of Sciences, Beijing 10039, China
*Corresponding author: aurelien.drezet@neel.cnrs.fr

Received 1 February 2018; revised 12 March 2018; accepted 12 March 2018; posted 23 March 2018 (Doc. ID 320403); published 13 April 2018

Based on the spin-dependent directional coupling of surface plasmons (SPs) by ∧-shaped antennas, ring-shaped structures built with such antennas have potential applications for optical tweezers and optical switch technology. In this Letter, we introduce an optical method for realizing a complete polarization tomography of coupled SP fields by such a chiral-planar structure. We use a far-field optical approach, namely leakage radiation microscopy (LRM), to map the SPs propagation and polarization. Here, we fully analyze the polarization state of the generated SPs inside the vortex lens structure. In addition, we provide a theoretical model which agrees well with the experimental results. © 2018 Optical Society of America

OCIS codes: (240.6680) Surface plasmons; (260.5430) Polarization; (050.4865) Optical vortices.

https://doi.org/10.1364/OL.43.001918

Optical angular momentum, including spin angular momentum (SAM) associated with polarization, and orbital angular momentum (OAM) associated with helical wave fronts, plays an important role in optical trapping, manipulation of micro-sized and nano-sized particles, and optical integrated devices [1–7]. Since surface plasmons (SPs) can overcome the diffraction limit and offer a promising approach to control and manipulate the propagation and the dispersion of light at the nanometer scale, the study of angular momentum in SPs becomes very attractive and important. Recently, studies in angular momentum in SPs have mainly focused on the spin sensitive intensity directionality (the so-called plasmonic spin Hall effect) [8–10], the OAM beam generation and measurements [11–17], as well as the desired polarization beam control [18,19]. A less-explored path, yet particularly important for application, is the polarization vector space character in the SPs field, especially in the vortex beam of the SPs.

Since plasmonic vortex lenses (PVL), like the ring-shaped structure of slit antennas [14], or Archimedean spiral groves [11], introduce the vortex-necessary azimuthal phase profile by controlling the spin-orbit coupling of photons with SPs, it becomes a typical way to generate an OAM beam in nano-optics. Among a variety of PVL designs, ∧-shaped or T-shaped slit antennas offer the possibility to set precisely the phase delay between two fixed dipoles, which lead to a strong spin-dependent coupling. Structures with ∧-shaped or T-shaped antennas have therefore attracted a lot of attention [8–10,14,19].

In this Letter, we show a complete polarization tomography for SPs characterizing the Stokes vector locally in the PVL. It is realized by means of a plasmonic imaging method called leakage radiation microscopy (LRM) [20] that can collect the leaked SPs propagating through the thin metal film and the substratum with a higher optical constant (usually glass) than the superstratum medium. This polarization tomography method is particularly important for applications in optical tweezers experiments in information processing [6,7] or in nanofluidics [4,5]. We apply the method to the ∧-shaped aperture design. Based on the local Stokes mapping, we reconstruct the polarization ellipses associated with the propagating SPs inside the structure. In addition, we provide a theoretical model reproducing experimental results.

We have previously reported that a ring structure based on ∧-shaped antenna with a 120-deg top angle between each slit is the optimal configuration for both directional coupling and singular SP generation [10]. Based on the ∧-shaped antenna's rotation direction, there are two types of ring-shaped PVL corresponding respectively to right-handed (i.e., clockwise) and left-handed (i.e., counterclockwise) geometries. These two enantiomers are related by in-plane mirror symmetries, which are also visible on the optical transmission properties. In this Letter, we restrict our investigation to the right-handed structure [Figs. 1(a) and 1(b)], which consist of 20 rotating ∧-shaped holes forming a 2–μm radius ring, each ∧ having two 200–nm-long, 50–nm-wide rectangular slits separated by a 120° apex angle. The structure is fabricated by a focused ion beam (FIB) milling on a thin Au layer with 50 nm in thickness, which satisfies the requirement for observing the SPs by LRM.

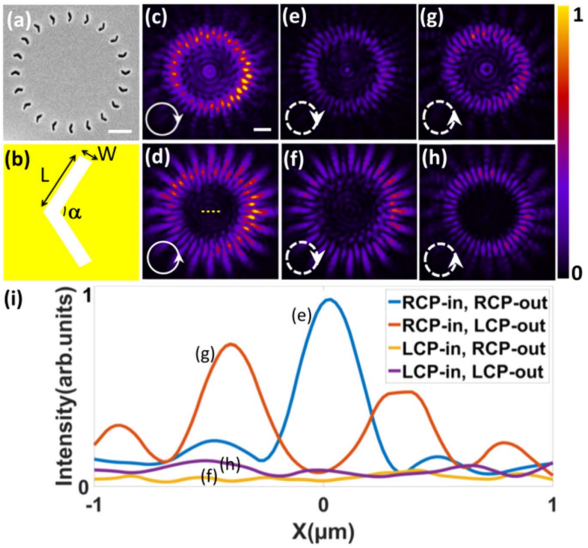

Fig. 1. (a) Electron micrograph of the right-handed geometry, with 2-μm ring radius. (b) Sketch of one ∧-shaped antenna with long $L = 200$ nm, wide $W = 50$ nm and apex peak $\alpha = 120°$. (c) and (d) Direct plane images under polarization excitation of (c) RCP and (d) LCP, respectively indicated by clockwise and counterclockwise solid arrows. (e) and (g) Signal recorded under RCP with polarization analysis indicated by the dotted arrows. (f) and (h) Signal recorded under LCP with polarization analysis. (i) Cross-section intensity profiles distribution along the horizontal line passing through the central region [corresponding to the yellow dotted line in Fig. 1(d)] of (e)–(h). The scale bars in (a) and (c) are 1 μm.

A far-field illumination and detection setup based on LRM is used [9] and the images are generated by illuminating the PVL [Fig. 1(a)] with an incoming right circularly polarized (RCP) [Fig. 1(c)] or left circularly polarized (LCP) [Fig. 1(d)] collimated He/Ne laser beam working at the 633–nm wavelength. The strong discrimination existing between the images obtained for the RCP input beam and the LCP input beam appears. Indeed, due to the spin-orbit interaction with the ∧-shaped apertures, the SPs beam is either inwardly or outwardly directed resulting in a very low signal inside the cavity for a LCP input state compared to the RCP input.

In order to quantitatively measure the spin-sensitive response of the SPs on the RCP and LCP excitations, signals recorded under the RCP [Figs. 1(e) and 1(f)] or LCP analysis [Figs. 1(g) and 1(h)] is performed and their cross-section profiles along an horizontal line through the center [corresponding to the yellow dotted line in Fig. 1(d)] are shown in Fig. 1(i). The extinction ratio that is used to quantify the singular SPs generation is calculated to be 11.78 based on the central peak values of Figs. 1(e) and 1(f). This reveals an excellent spin-dependent directional intensity character and is consistent with the conclusion in [10] in which the same PVL structure, i.e., with identical geometrical parameters was used. However, in the whole view, the SPs intensities for the LCP excitation showed in Fig. 1(i) are relatively much weaker compared with the coupled SPs for the RCP excitation light. This shows the optimal outwardly directional character. As explained in [21], the quality of the LRM images is strongly dependent on the focusing of the oil immersion objective. Here, we carefully adjust the position of the oil immersion objective to make it reaching the best focusing position it could.

In order to describe the polarization distribution of the induced SPs beams, we use Stokes parameters (S_0, S_1, S_2, S_3) [22], which are calculated at each image point by combining six measured intensities ($I_{\hat{X}}$, $I_{\hat{Y}}$, $I_{\hat{P}}$, $I_{\hat{M}}$, $I_{\hat{R}}$, $I_{\hat{L}}$) corresponding to the projections of the induced SPs along six different polarization analysis directions. $\hat{X}$, $\hat{Y}$, $\hat{P}$, $\hat{M}$, $\hat{R}$, and $\hat{L}$ are the unit polarization vectors along, respectively, the 0°, 90°, 45°, 135°, RCP, and LCP directions. Here, we use the notation $\hat{P} = (\hat{X} + \hat{Y})/\sqrt{2}$, $\hat{M} = (\hat{X} - \hat{Y})/\sqrt{2}$, $\hat{R} = (\hat{X} - i\hat{Y})/\sqrt{2}$, $\hat{L} = (\hat{X} + i\hat{Y})/\sqrt{2}$. The Stokes parameters are related to ($I_{\hat{X}}$, $I_{\hat{Y}}$, $I_{\hat{P}}$, $I_{\hat{M}}$, $I_{\hat{R}}$, $I_{\hat{L}}$) are as follows:

$$S_0 = I_{\hat{X}} + I_{\hat{Y}} = I_{\hat{P}} + I_{\hat{M}} = I_{\hat{R}} + I_{\hat{L}} = I, \quad (1)$$

$$S_1 = I_{\hat{X}} - I_{\hat{Y}} = p \cos 2\varphi \cos 2\chi I, \quad (2)$$

$$S_2 = I_{\hat{P}} - I_{\hat{M}} = p \sin 2\varphi \cos 2\chi I, \quad (3)$$

$$S_3 = I_{\hat{R}} - I_{\hat{L}} = p \sin 2\chi I, \quad (4)$$

where I is the total intensity of the beam, and p is the degree of the polarization constrained by $0 \le p \le 1$. 2φ and 2χ are the spherical angles defining the direction of the Stokes vector on the Poincare sphere.

In order to get the set of six required intensity maps, we use a polarizer and a quarter wave plate located after the oil immersion objective to set the polarization projection in the direction of $\hat{X}$, $\hat{Y}$, $\hat{P}$, $\hat{M}$, $\hat{R}$, and $\hat{L}$. Considering the strong transmission of the incident beam near the ∧-shaped geometries, we focus our attention on the central area of the PVL where the SPs signature dominates. The LRM images analyzed along various polarizations are shown in Figs. 2(a)–2(g) where Fig. 2(a) corresponds to the total transmitted intensity, while Figs. 2(b)–2(g) show the projected intensity distribution along the different polarization directions: $\hat{X}$, $\hat{Y}$, $\hat{P}$, $\hat{M}$, $\hat{R}$, and $\hat{L}$.

At the same time, an analytical simulation for these six intensity maps in the PVL has been obtained based on the multi-dipolar model discussed in Ref. [10]. The in plane electric field vector near the structure center is in this model given by

$$\vec{E} \propto C_\sigma [e^{i(\sigma+1)\theta_M} J_{\sigma+1}(k_{SP} r_M)\vec{E}_{-1} + e^{i(\sigma-1)\theta_M} J_{\sigma-1}(k_{SP} r_M)\vec{E}_{+1}], \quad (5)$$

where M is the observation point expressed using polar coordinates θ_M and r_M. k_{SP} is the wave vector of the induced SPs, and $\vec{E}_{-1}$ and $\vec{E}_{+1}$ are, respectively, the unit electric fields of the RCP and LCP states. In addition, σ denotes the circular polarization state of the incident beam (i.e., $\sigma = 1$ or $\sigma = -1$ for LCP and RCP incident states), and C_σ refers to the SPs coupling efficiency, which relates to the plasmonic structure. Meanwhile, $J_{\sigma\pm1}$ refers to the $(\sigma \pm 1)^{th}$ order Bessel function. When $\sigma = \pm 1$, the resultant SP polarization analysis intensity could be represented by J_0^2 and $J_{\pm2}^2$.

After calculating the total SPs intensity I corresponding to an RCP incident light (i.e., $\sigma = -1$) coupled with our structure, we project the field along the $\hat{X}$, $\hat{Y}$, $\hat{P}$, $\hat{M}$, $\hat{R}$, and $\hat{L}$ directions and show the theoretical intensity maps I, $I_{\hat{X}}$, $I_{\hat{Y}}$, $I_{\hat{P}}$, $I_{\hat{M}}$, $I_{\hat{R}}$, and $I_{\hat{L}}$ in Figs. 2(h)–2(n).

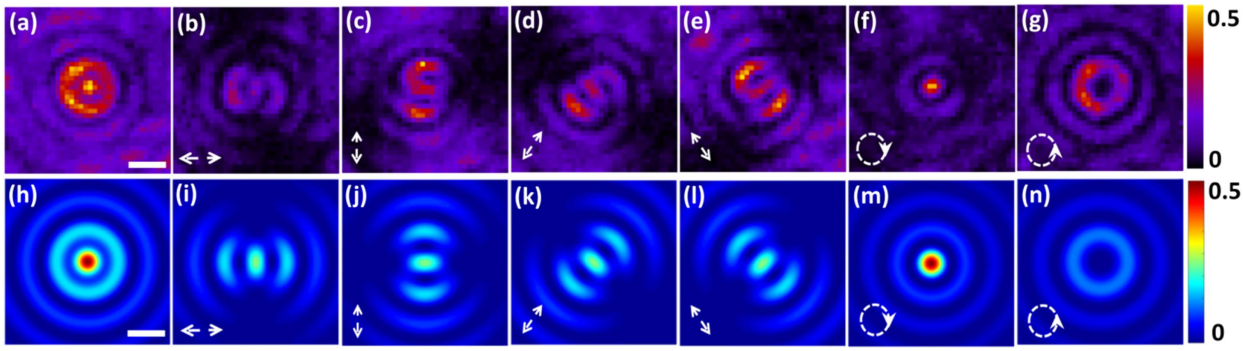

Fig. 2. Experimental results (a)–(g) and simulation results (h)–(n) for RCP incident beam with total intensity (a), (h) and $\hat{X}$, $\hat{Y}$, $\hat{P}$, $\hat{M}$, $\hat{R}$, $\hat{L}$ direction polarizations analyses (b)–(g), (i)–(n) indicated by the dotted arrows. The scale bars in (a) and (h) are 0.5 μm.

The comparison between the simulations and the experiments reveals an excellent agreement demonstrating the effectiveness of our approach.

Based on Eqs. (1)–(4), Stokes vectors are calculated for both the experiment [Figs. 3(a)–3(d)] and the theory [Figs. 3(e)–3(h)]. A good agreement is found. As it can be seen the, S_3 distributions obtained from experiment [Fig. 3(d)] and from the theory [Fig. 3(h)] are roughly similar. Importantly, the central zone of the S_3 map reveals a maximum value while, S_1, and S_2 in Figs. 3(b), 3(c), 3(f), and 3(g) show a near-zero value in the same zone (we point out a small discrepancy between Figs. 3(b) and 3(f) attributed to an optical misalignment). This implies that the SPs field is in a nearly pure RCP state in this zone.

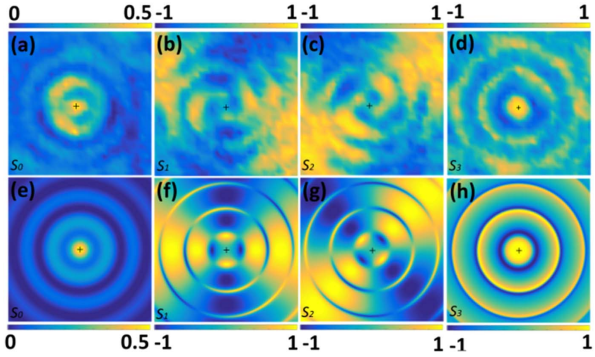

Fig. 3. Normalized Stokes parameters (S_0, S_1, S_2, S_3) calculated based on Fig. 2 for experimental results (a)–(d) and simulation results (e)–(h), respectively.

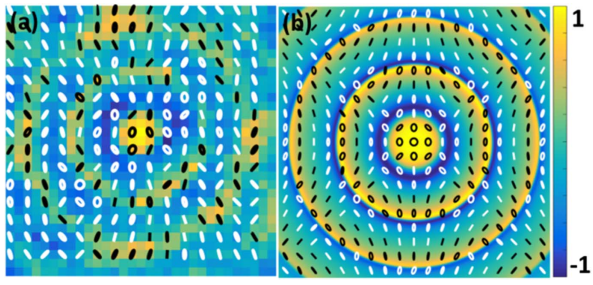

Fig. 4. Polarization tomography for experimental (a) and theoretical results (b) on the S_3^* map of Figs. 3(d) and 3(h). In these maps, a white (respectively black) color ellipse corresponds to the left-handed (respectively right-handed).

From the Stokes vectors and Eqs. (1)–(4), we can extract the polarization ellipse parameters p, φ, and χ, and thus complete the tomography procedure for the PVL structure. For a good comparison, we superpose for both the experiment [Fig. 4(a)] and the theory [Fig. 4(b)] the reconstructed polarization ellipses on the S_3 maps of Fig. 3(d) and Fig. 3(h) taken as background. Figure 4 is a spatial mapping of the local SP field. It is visible that the polarization ellipse at the center is associated with a quasi-pure RCP state, and this is fully consistent with the previous analysis obtained directly from the Stokes vectors.

In summary, based on a mapping of the local Stokes parameters with LRM, we developed a complete polarization tomography method for SPs fields. This method allows a precise mapping of the polarization ellipse inside any planar plasmonic device, which could have many applications. We applied this protocol to the ring-shaped PVL based on the ∧-shaped antennas. The experimental and theoretical analysis demonstrate that the right-handed structure coupling with RCP states of light can produce a nearly pure RCP SP state in the center of the structure. In contrast, the illumination with the LCP shows a weak residual signal, which is a direct signature of the spin orbit coupling of light with the SPs in such a device. We believe that such systems coupled to the complete polarization tomography proposed here offer interesting perspective for information encoding using the SPs and the optical vortices.

Funding. Agence Nationale de la Recherche (ANR) (ANR-13-BS10-0007).

Acknowledgment. We thank J.-F. Motte and G. Julie, from NANOFAB facility in Neel Institute, for sample fabrication. The PhD grant of A. Zhao by China Scholarship Council and of A. Pham by the Ministère de la Region Rhone-Alpes are gratefully acknowledged.

REFERENCES

1. M. E. J. Friese, T. A. Nieminen, N. R. Heckenberg, and H. Rubinsztein-Dunlop, Opt. Lett. **23**, 1 (1998).
2. K. T. Gahagan and G. A. Swartzlander, Opt. Lett. **21**, 827 (1996).
3. D. G. Grier, Nature **424**, 810 (2003).
4. L. Tong, V. D. Miljkovic, and M. Kall, Nano Lett. **10**, 268 (2010).

5. M. L. Juan, M. Righini, and R. Quidant, Nat. Photonics **5**, 349 (2011).
6. B. Guan, R. P. Scott, C. Qin, N. K. Fontaine, T. Su, C. Ferrari, M. Cappuzzo, F. Klemens, B. Keller, M. Earnshaw, and S. J. B. Yoo, Opt. Express **22**, 145 (2014).
7. D. Dai, L. Liu, S. Gao, D.-X. Xu, and S. He, Laser Photon. Rev. **7**, 303 (2012).
8. J. Lin, J. P. B. Mueller, Q. Wang, G. Yuan, N. Antoniou, X.-C. Yuan, and F. Capasso, Science **340**, 331 (2013).
9. Q. Jiang, A. Pham, M. Berthel, S. Huant, J. Bellessa, C. Genet, and A. Drezet, ACS Photon. **3**, 1116 (2016).
10. Q. Jiang, A. Pham, J. Bellessa, S. Huant, C. Genet, and A. Drezet, Opt. Lett. **41**, 4534 (2016).
11. H. Kim, J. Park, S.-W. Cho, S.-Y. Lee, M. Kang, and B. Lee, Nano Lett. **10**, 529 (2010).
12. P. Genevet, N. Yu, F. Aieta, J. Lin, M. A. Kats, R. Blanchard, M. O. Scully, Z. Gaburro, and F. Capasso, Appl. Phys. Lett. **100**, 013101 (2012).
13. P. Zilio, G. Parisi, D. Garoli, M. Carli, and F. Romanato, Opt. Lett. **39**, 4899 (2014).
14. P. Li, S. Liu, C. Ma, L. Han, H. Cheng, and J. Zhao, Opt. Lett. **41**, 2205 (2016).
15. F. Huang, X. Jiang, H. Yuan, and X. Sun, Plasmonics **12**, 751 (2017).
16. A. P. Liu, X. Xiong, X.-F. Ren, Y.-J. Cai, G.-H. Rui, Q.-W. Zhan, G.-C. Guo, and G.-P. Guo, Sci. Rep. **3**, 2402 (2013).
17. R. Chen, X. Zhang, Y. Zhou, H. Ming, A. Wang, and Q. Zhan, Appl. Opt. **56**, 4868 (2017).
18. A. Pors and S. I. Bozhevolnyi, Opt. Express **21**, 2942 (2013).
19. L.-J. Black, Y. Waang, C. H. de Groot, A. Arbouet, and O. L. Muskens, ACS Nano **8**, 6390 (2014).
20. A. Drezet, A. Hohenau, D. Koller, A. Stepanov, H. Ditlbacher, B. Steinberger, F. R. Aussenegg, A. Leitner, and J. R. Krenn, Mater. Sci. Eng. B **149**, 220 (2008).
21. M. Berthel, Q. Jiang, C. Chartrand, J. Bellessa, S. Huant, C. Genet, and A. Drezet, Phys. Rev. E **92**, 033202 (2015).
22. M. Born and E. Wolf, *Principles of Optics*, 7th (expanded) ed. (Cambridge University, 1999).

159.226.165.17 [as 2019-08-14 22:42:47]